



7N-25-1R

NASA-CR-201428

AIAA 94-0686

**A Theoretical Evaluation of
Secondary Atomization Effects on
Engine Performance for Aluminum
Gel Propellants**

D.C. Mueller and S.R. Turns

**The Pennsylvania State University
University Park, PA**

**32nd Aerospace Sciences
Meeting & Exhibit
January 10-13, 1994 / Reno, NV**

A Theoretical Evaluation of Secondary Atomization Effects on Engine Performance for Aluminum Gel Propellants

Donn C. Mueller[†] and Stephen R. Turns[‡]
 The Pennsylvania State University
 University Park, PA, 16802

Abstract

A one-dimensional model of a gel-fueled rocket combustion chamber has been developed. This model includes the processes of liquid hydrocarbon burnout, secondary atomization, aluminum ignition, and aluminum combustion. Also included is a model of radiative heat transfer from the solid combustion products to the chamber walls. Calculations indicate that only modest secondary atomization is required to significantly reduce propellant burnout distances, aluminum oxide residual size and radiation heat losses. Radiation losses equal to approximately 2-13 % of the energy released during combustion were estimated. A two-dimensional, two-phase nozzle code was employed to estimate radiation and nozzle two-phase flow effects on overall engine performance. Radiation losses yielded a 1 % decrease in engine I_{sp} . Results also indicate that secondary atomization may have less effect on two-phase losses than it does on propellant burnout distance and no effect if oxide particle coagulation and shear induced droplet breakup govern oxide particle size. Engine I_{sp} was found to decrease from 337.4 to 293.7 seconds as gel aluminum mass loading was varied from 0-70 wt%. Engine I_{sp} efficiencies, accounting for radiation and two-phase flow effects, on the order of 0.946 were calculated for a 60 wt% gel, assuming a fragmentation ratio of 5.

Nomenclature

a-	absorption coefficient
A-	area
c_p -	specific heat
C_D -	drag coefficient
d-	diameter
$F_n(T)$ -	fraction of total radiation emitted by a blackbody at temperature T in the wavelength interval n
h-	average convective heat transfer coefficient
i-	specific enthalpy
I-	radiant intensity
I_0, I_1 -	modified Bessel functions
j-	droplet size class
k-	thermal conductivity
L-	number of wavelength intervals
m-	mass
\dot{m} -	droplet mass flux or mass flux through the combustion chamber
M-	number of droplet size classes
n-	wavelength interval

Nu-	Nusselt number
N/τ -	number of droplets passing through combustor control volume per unit time
r_s -	droplet/particle surface radius
r-	radial coordinate/position in terms of optical thickness
R-	chamber radius
R -	chamber radius in terms of optical thickness
q^f -	radiation heat flux from condensed combustion products to wall
t-	time
T-	temperature
u_p -	particle velocity
x-	axial location in the combustor model

Greek

α_1, α_2 -	control switches
β -	fragmentation ratio (number of secondary droplets produced per initial droplet)
ϕ -	angular coordinate
η -	fraction of aluminum droplet mass that forms as Al_2O_3 residual on droplet surface
λ -	wavelength
ρ -	density
σ -	Stefan-Boltzmann constant
σ_s -	scattering coefficient
θ -	angular coordinate
Ω_o -	scattering albedo

Subscripts

Al-	aluminum
b-	boiling, propellant burnout, or blackbody
f-	aluminum oxide fume particles or aluminum flame
fg-	liquid-gas
g-	gas
LH-	liquid hydrocarbon
o-	initial
Ox-	Aluminum oxide residual
p-	particle/droplet
w-	wall

Introduction

Gel propellants, in which fine particles are suspended in a gelled combustible liquid, offer potential performance and/or safety advantages over conventional liquid and

[†] Graduate Assistant, Student Member, AIAA

[‡] Professor, Mechanical Engineering
 Member, AIAA

solid propellants in rocket applications. Theoretical performance evaluations show that gel propellants may provide increases in specific impulse (I_{sp}) and/or propellant density over conventional liquid propellants.¹⁻⁷ A number of potential liquid/solid constituent combinations were theoretically evaluated over a range of mixture ratios and solid constituent loadings for use in a LEO-GEO mission with fixed propellant tankage volume and vehicle dry-mass with no limit on initial gross mass.⁷ Based on propellant toxicity and vehicle payload considerations, aluminum was predicted to be the best candidate solid constituent.

More detailed analyses of earth-to-LEO, LEO-to-GEO, LEO-to-Moon, LEO-to-Mars, and several planetary fly-by missions, incorporating appropriate total vehicle mass/volume limitations and propellant density effects on vehicle dry-mass, also were performed to compare various aluminum gels with their liquid bi-propellant counterparts.³⁻⁶ These studies indicate that gel propellants are likely to provide the greatest benefit on earth-to-LEO, and high-energy planetary missions with NTO/MMH/Al gels also providing significant performance gains over NTO/MMH in LEO-to-GEO and LEO-to-Moon missions. For example, replacing the space shuttle solid boosters with an RP-1/O₂/Al or NTO/MMH/Al propellant combination, while maintaining the same booster dimensions, could theoretically increase maximum payload by 14-35% over the current shuttle payload.⁶ Similarly, the addition of aluminum to nitrogen tetroxide/ monomethyl hydrazine (NTO/MMH) may permit planetary missions that would be impossible with neat NTO/MMH.⁵

In the area of propellant rheology, recent gains have been made in the development of stable gels that are easily sprayed,⁸⁻¹⁰ but more work in this area is still required. In related work, testing has demonstrated that expulsion pumping is feasible in a small engine system and that gel-fueled engines can be throttled over a range of operating conditions, shut-down, and restarted as desired.¹¹ In addition, experimental results indicate that using aluminum can reduce combustion instabilities associated with liquid hydrocarbon propellants.²

Although the above investigations are promising, it should be noted that the theoretical performance studies¹⁻⁷ do not incorporate I_{sp} losses associated with aluminum combustion such as increased propellant combustion times, radiation heat transfer from condensed combustion products to the chamber walls, and nozzle two-phase flow losses due to these same condensed products. Because I_{sp} efficiency losses of only 1.5-4% may be sufficient to eliminate the payload benefits of using aluminum gels, minimization of aluminum combustion related losses is desirable. In addition, these performance losses must be determined before the performance of gel propellants can be accurately evaluated.

Since previous work^{12,13} has shown that the individual aluminum particles in a gel droplet can form an agglomerate that burns as a single aluminum droplet, it is apparent that small gel droplets are beneficial in reducing performance losses. Fine atomization of gel propellants, however,

can be difficult to achieve due to their viscous nature. Fortunately, secondary atomization,¹⁴⁻¹⁹ in which a droplet spontaneously shatters into a number of smaller droplets due to internal vaporization of the liquid carrier, may produce the desired small droplets.

Although secondary atomization has been proposed as a means of reducing gel-related performance losses, previous research has focused on the secondary atomization mechanism itself rather than its effects on engine performance. The focus of our present investigation, therefore, is to theoretically examine the effects of secondary atomization on engine performance losses and, incorporating these performance loss estimates, evaluate the performance potential of gel-fueled engines. To accomplish these objectives, a one-dimensional combustor model has been derived to evaluate secondary atomization effects on propellant burnout distances and radiation heat losses in a rocket combustion chamber. This combustor code is used in conjunction with the Solid Propellant Rocket Motor Performance Prediction Computer Program (SPP),²⁰ a two-dimensional, two-phase rocket code, to provide a preliminary evaluation of nozzle two-phase flow losses and overall engine performance.

Combustion Chamber Model

One-Dimensional Model Description

In brief, a radially uniform spray, consisting of four droplet size classes, enters the combustion chamber and burns in a process incorporating liquid carrier burnout, droplet secondary atomization, aluminum agglomerate heat-up and combustion, two-phase particle flow, and radiation heat transfer from solid combustion products to the chamber walls. The propellants used in the combustor model are a JP-10/Al gel and a preheated gaseous O₂ oxidizer. JP-10, a pure hydrocarbon (C₁₀H₁₆), was chosen as the gel hydrocarbon component instead of RP-1 to avoid the complexity of modeling multi-component droplet combustion. The combustor flow is modeled using a single product-phase containing both gases and small Al₂O₃ fume particles, and three additional flow phases for each droplet size class: a liquid hydrocarbon phase, an aluminum phase, and a phase containing large Al₂O₃ residuals. The Al₂O₃ must be separated into two flow phases because of the two oxidation mechanisms inherent in aluminum combustion.^{21,22} In the first oxidation mechanism, large Al₂O₃ residuals are formed through droplet surface condensation/oxidation, and in the second, very small Al₂O₃ fume particles are produced through vapor-phase oxidation. Since the Al₂O₃ residuals are much larger than the fume particles and are attached to the surface of the aluminum droplets it is necessary to model the Al₂O₃ residuals separately from the fume particles. Including the fume particles in the gas-phase flow requires the assumptions of no temperature or velocity slip between the fume particles and the gases, which are reasonably valid, and greatly simplifies the problem solution.

As an Al droplet burns, it continually produces Al₂O₃ fume particles at the oxide boiling point which subse-

quently equilibrate with the gas-phase temperature and velocity. This process results in a range of fume particle temperatures and velocities as new particles are created and older particles continue to equilibrate with the gases. If the temperature and velocity slip were not neglected, many additional flow phases would be required to accurately model this range of fume particle temperatures and velocities.

Mass Conservation: Using the definition of velocity, $u = dx/dt$, to relate the differential variables, dx and dt , the following equation can be written for system mass conservation for M droplet size classes:

$$\frac{dm_g}{dx} = - \sum_{j=1}^M \left[\frac{N}{\tau} \frac{1}{u_{p,j}} \left(\frac{dm_{d,LH}}{dt} + \frac{dm_{d,Al}}{dt} + \frac{dm_{d,Ox}}{dt} \right) \right] \quad (1)$$

where it is assumed that no mass is added to or removed from the chamber except at the injector face and the chamber exit, and that steady-state operation prevails.

The three time derivatives on the right hand side of Eq. 1 are found from hydrocarbon droplet gasification and aluminum droplet combustion models which are discussed later in this paper. The value of N/τ_j for each droplet size class can be determined from the total initial gel mass flux and a normalized droplet size distribution.

Energy Conservation: The steady-state energy balance for the system, including radiation heat losses, can be expressed as

$$\frac{d(mi)_g}{dx} = - \sum_{j=1}^M \left[\frac{d(mi)_{LH}}{dx} + \frac{d(mi)_{Al}}{dx} + \frac{d(mi)_{Ox}}{dx} \right] - 2\pi Rq_r \quad (2)$$

Since gas flow optical properties are dominated by the small Al_2O_3 fume particles,²³ the radiation term is independent of the individual droplet size classes and is not included in the summation term. Each of the terms on the right hand side of Eq. 2 can be represented as follows by expanding the derivatives and assuming that the only changes in specific enthalpy are due to convective heat transfer with the gaseous product-phase:

$$\frac{d(mi)_j}{dx} \Big|_j = \left[\frac{N}{\tau} \frac{1}{u_p} \left(\alpha_1 \dot{m} \frac{A_p h (T_g - T_p)}{m_p} + \alpha_2 i \frac{dm_p}{dt} \right) \right] \quad (3)$$

The coefficients α_1 and α_2 , equal to 0 or 1, are used to provide the correct terms, depending on whether the liquid hydrocarbon, aluminum, or Al_2O_3 mass flux is being examined. In the hydrocarbon vaporization model, the bulk droplet temperature is assumed to remain at the initial droplet temperature while only a thin surface layer of hy-

drocarbon is heated to the hydrocarbon boiling temperature before being vaporized. Since the liquid hydrocarbon enthalpy does not vary with chamber axial location, $\alpha_1=0$ and $\alpha_2=1$. In this case, the enthalpy, i , equals the initial liquid hydrocarbon specific enthalpy, and dm_p/dt is the hydrocarbon mass vaporization rate from a single droplet.

Following hydrocarbon burnout, an agglomerate of aluminum particles remains.^{12,13} The aluminum agglomerate temperature rises from the hydrocarbon boiling temperature, through the aluminum melting point, to the aluminum ignition temperature as heat is transferred from the gas flow to the agglomerate, at which point aluminum combustion commences. In the combustor model, this agglomerate ignition/heat-up process is approximated as convective heat transfer from the gas flow to a spherical, uniform-temperature agglomerate. Heat transfer to the agglomerate causes the agglomerate temperature to rise from the hydrocarbon boiling temperature to the aluminum melting temperature. The agglomerate temperature is then held constant until sufficient energy to melt the entire agglomerate has been transferred from the gas-flow, at which point it is assumed that aluminum combustion begins. Heat-up of the molten aluminum droplet to the aluminum boiling temperature is accounted for in the aluminum combustion model, as discussed below. Since it is assumed that no aluminum vaporization occurs during agglomerate heat-up and melting, and because the specific enthalpy does change, $\alpha_1=1$ and $\alpha_2=0$ during these stages of the aluminum ignition/combustion process. Once the agglomerate melts, however, the aluminum specific enthalpy remains constant for the same reasons as discussed for the liquid hydrocarbon, and combustion begins to occur. During this portion of the ignition/combustion process, $\alpha_1=0$, $\alpha_2=1$, and the specific enthalpy, i , equals that of liquid aluminum at its melting temperature.

Since the Al_2O_3 residual forms on the aluminum droplet surface, the Al_2O_3 residual is maintained at the aluminum boiling temperature, and therefore maintains a constant specific enthalpy, as long as any aluminum remains in the droplet. For the time period prior to aluminum burnout, $\alpha_1=0$, $\alpha_2=1$, and the specific enthalpy is that of Al_2O_3 at the aluminum boiling temperature. Once aluminum combustion and Al_2O_3 formation ceases, $\alpha_1=1$, $\alpha_2=0$, and the particle temperature is allowed to equilibrate with the gas temperature. The total system energy balance is represented by the substitution of Eq. 3 with appropriate values of α_1 , α_2 , and i into Eq. 2.

Radiation Heat Transfer: Radiation from the solid combustion products to the chamber walls is a participating media phenomenon, requiring a solution of the radiative transfer equation.²⁴ Expressed in cylindrical coordinates this equation is

$$\sin\theta \left[\cos\phi \frac{\partial I}{\partial r} - \frac{\sin\phi}{r} \frac{\partial I}{\partial \phi} \right] + I = \quad (4)$$

$$(1 - \Omega_0) I_{b,r}(r) + \frac{\Omega_0}{4\pi} \iint I \sin\theta' d\theta' d\phi'$$

where $I=I(r,\theta,\phi)$. It should be noted that the radial position, r , is based on optical thickness and is not a physical position (i.e., $r = \int (a + \sigma_s) dr$). The scattering albedo, Ω_0 is defined as

$$\Omega_0 = \frac{\sigma_s}{a + \sigma_s} \quad (5)$$

where a and σ_s are determined from Mie theory. In the Mie scattering calculations the fume particles are assumed to be uniform in size (1 μm), and the refractive indices are those of Al_2O_3 smoke.²³

Since the flow is likely to be optically thick,^{23,25} a cylindrical P_1 diffusion approximation is used to simplify the radiative transfer equation. By assuming that $I_{b,r}$ is independent of radial location, the following equation for radiative heat flux is obtained:²⁵

$$q^r(R) = \int \frac{4\pi I_1\left(\frac{R}{\xi}\right) (I_{b,r} - I_{b,w})}{3\xi I_0\left(\frac{R}{\xi}\right) + 2I_1\left(\frac{R}{\xi}\right)} d\lambda. \quad (6)$$

The variable ξ is based on the flow optical properties and is defined as

$$\xi = \frac{1}{\sqrt{3(1 - \Omega_0)}} \quad (7)$$

If $\xi(\lambda)$ is assumed to be constant over a wavelength interval, Eq. 6 can be expressed as the following summation:

$$q^r(R) = \sum_{n=1}^L \frac{4I_1\left(\frac{R}{\xi}\right)_n}{3\xi_n I_0\left(\frac{R}{\xi}\right)_n + 2I_1\left(\frac{R}{\xi}\right)_n} \cdot \{F_n(T_g)\sigma T_g^4 - F_n(T_w)\sigma T_w^4\} \quad (8)$$

Momentum Conservation: The gas-phase momentum equation in the combustion chamber is trivial assuming a negligible chamber pressure gradient and no body forces. Neglecting virtual mass and Bassett forces, the particle momentum equation for a given droplet size class can be expressed as

$$\frac{du_p}{dx} = \frac{3\rho_g C_D (u_g - u_p) |u_g - u_p|}{4\rho_p d_p u_p} \quad (9)$$

Gel Combustion and Secondary Atomization: The physics of gel droplet combustion and probable secondary atomization processes are described in other work.¹²⁻¹⁹ In the present model, rigid-shell induced secondary atomization¹⁷⁻¹⁹ is assumed. In the combustor code, secondary atomization is presumed to occur when the droplet diameter reaches the predicted rigid-shell diameter. Although secondary atomization actually occurs some time after rigid shell formation, the time interval is currently unknown and is therefore neglected in the combustor model. Particle size distribution after secondary atomization is also presently unknown and is treated as a system variable. In the combustor model, a droplet undergoing secondary atomization is assumed to shatter into a specified number of equal-size secondary droplets. Defining the fragmentation ratio, β , as the number of secondary droplets produced per initial droplet, a new value of N/τ_j can be expressed as

$$\frac{N}{\tau} \Big|_{j,\text{new}} = \beta \frac{N}{\tau} \Big|_{j,\text{old}} \quad (10)$$

Equation 10 is then used to determine a new droplet diameter, d_j , given the gel mass flux of the j^{th} size class.

Hydrocarbon Vaporization: Based on the relative proximity of the gel droplets to each other, it is unlikely that the droplets are surrounded by individual flames. Therefore, hydrocarbon combustion is represented using a spherically symmetric droplet evaporation model with convective effects incorporated through film theory.²⁶ As mentioned previously, droplet heat up is approximated by assuming that heat transfer from the gas flow only affects a thin liquid layer at the droplet surface. Assuming quasi-steady, spherically symmetric droplet vaporization with unity Lewis number, uniform droplet temperature, and constant thermophysical properties, the hydrocarbon vaporization rate can be expressed as

$$\frac{dm_{d,LH}}{dt} = -\frac{2\pi k_g Nu r_s}{c_{p,g}} \ln \left[\frac{c_{p,g} (T_g - T_{b,LH})}{i_{fg} + \int_{T_0}^{T_b} c_{p,LH} dT} + 1 \right] \quad (11)$$

Aluminum Combustion: As mentioned previously, aluminum combustion proceeds through two oxidation mechanisms: aluminum vapor oxidation and droplet surface condensation/oxidation. This aluminum combustion process is treated using a simple combustion model in which a specified fraction of the vaporizing aluminum is involved in the surface oxidation/condensation mechanism. It is assumed that all heat released by this surface mechanism goes into the droplet with none lost to the sur-

rounding gases. Using the same assumptions as the hydrocarbon model and assuming that Al_2O_3 does not interfere with aluminum vaporization, the droplet vaporization rate can be expressed as

$$\frac{dm_{d,Al}}{dt} = -\frac{2\pi k_g \text{Nu} r_s}{c_{p,g}} \left[\frac{c_{p,g}(T_f - T_{b,Al})}{i_{fg,Al} + \int_{T_{m,Al}}^{T_{b,Al}} c_{p,Al} dT - \eta i_{fg,Ox}} + 1 \right] \quad (12)$$

It should be noted that i_{fg,Al_2O_3} is not a true enthalpy of vaporization since Al_2O_3 does not exist in a vapor state. Therefore, i_{fg,Al_2O_3} is actually the enthalpy change for the chemical reaction, $2\text{Al}_{(g)} + 3/2\text{O}_{2(g)} \rightarrow \text{Al}_2\text{O}_{3(l)}$, occurring at the droplet surface temperature. Droplet lifetime comparisons with an empirical correlation for aluminum droplet combustion in solid rockets²⁰ demonstrated good agreement. Average thermophysical properties are estimated as recommended in previous droplet combustion work.²⁷

Solution Method: Equations 1,2,9,11, and 12 form the governing equation set and are numerically integrated in the axial direction using the IMSL Dverk integration routine.²⁸ Gas-phase temperature, density, and composition are calculated using the STANJAN chemical equilibrium subroutine.²⁹ The temperature dependent gas-phase conductivity and viscosity are approximated as those of O_2 to avoid the complexities of calculating gas mixture properties. Details of these and other properties used in the combustor model can be found in reference 30.

One-Dimensional Combustor Model Results

The one-dimensional combustor code was exercised using the conditions presented in Table 1. These values were chosen to simulate an upper-stage booster and represent the maximum I_{sp} operating point for a 60 wt% aluminum gel. Because propellant mass flow rate in a rocket is governed in part by nozzle geometry, the SPP nozzle code²⁰ was used to determine the propellant mass flow rates. Since an appropriate spray distribution remains to be determined from gel atomization research, the arbitrary normalized droplet size distribution presented in Fig. 1 was used.

Gas temperature and composition, assuming a frag-

Table 1. Model Operating Conditions	
Chamber Diameter	0.19 m
Chamber Pressure	38 atm
Liquid Carrier	JP-10
Gel Aluminum Loading	60%
Gel Flow Rate	10.78 kg/s
Oxidizer Flow Rate	11.75 kg/s

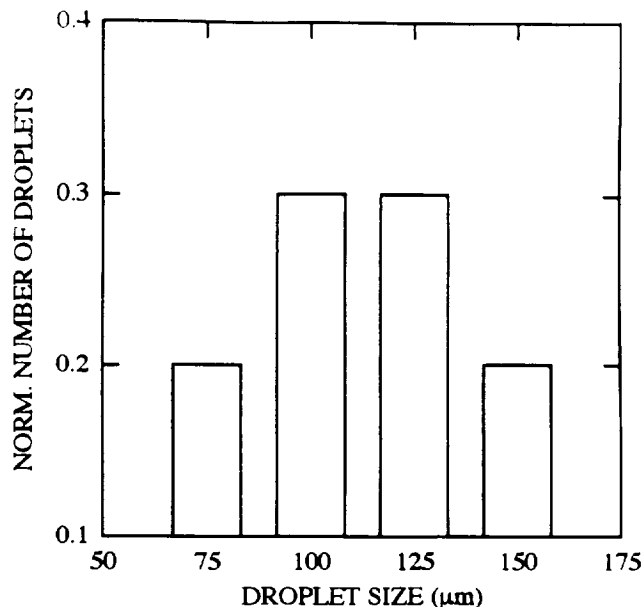


Figure 1. Normalized droplet size distribution used in the combustor code.

mentation ratio, β , of 5 are presented in Fig. 2. The jagged shapes of both the temperature and composition profiles arises from using only four droplet size classes instead of a continuous droplet size distribution. The slow rate of temperature increase in the region between 0.1 and 0.25 m is caused by the large enthalpy transfer from the gas flow to heat the aluminum after hydrocarbon burnout.

In Fig. 3, propellant burnout distance is plotted versus fragmentation ratio, β , to illustrate the potential benefits of

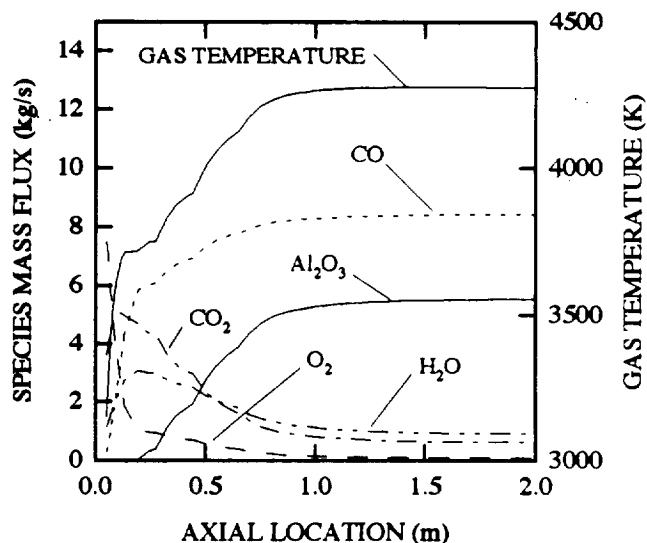


Figure 2. Gas temperature and major species mass fluxes versus axial location. Data are for a 60 wt% aluminum gel assuming a fragmentation ratio of 5.

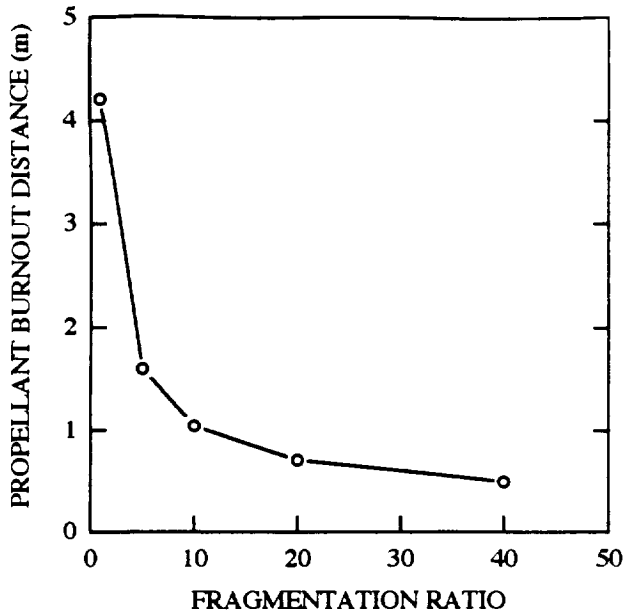


Figure 3. Propellant burnout distance as a function of secondary atomization fragmentation ratio for a 60 wt% aluminum gel.

secondary atomization in reducing required engine residence times. It is readily apparent that only slight secondary atomization is required to significantly reduce propellant burnout distance, and that higher secondary atomization intensities, represented by larger fragmentation ratios, have a lesser marginal effect, primarily due to the fact that droplet lifetime is inversely proportional to droplet surface area, which increases as $(\beta)^{2/3}$.

Final oxide residual diameter as a function of fragmentation ratio is shown in Fig. 4. Similar to the trend seen in propellant burnout, small secondary atomization intensities significantly reduce final Al_2O_3 residual diameter, with greater atomization intensities providing decreasing marginal reductions in residual diameter. Final residual particle diameter, however, is proportional to $(1/\beta)^{1/3}$ instead of $(1/\beta)^{2/3}$ as is droplet lifetime.

Radiation losses from condensed combustion products to the chamber walls as functions of fragmentation ratio and aluminum mass loading are shown in Fig. 5. Chamber operating conditions are those that produce maximum I_{sp} for each aluminum loading. Radiation losses were found to be strongly influenced by the fragmentation ratio, primarily due to changes in propellant burnout distance. Increasing the gel aluminum mass loading for a given fragmentation ratio was also found to increase radiation losses because of increased chamber temperature and slight increases in propellant burnout distance with increasing aluminum mass loading. Radiation losses were approximately equal to 2-13% of the energy released during combustion, depending on the aluminum mass loading and fragmentation ratio.

It should be cautioned that the above radiation heat transfer calculations are only approximate. Axial radia-

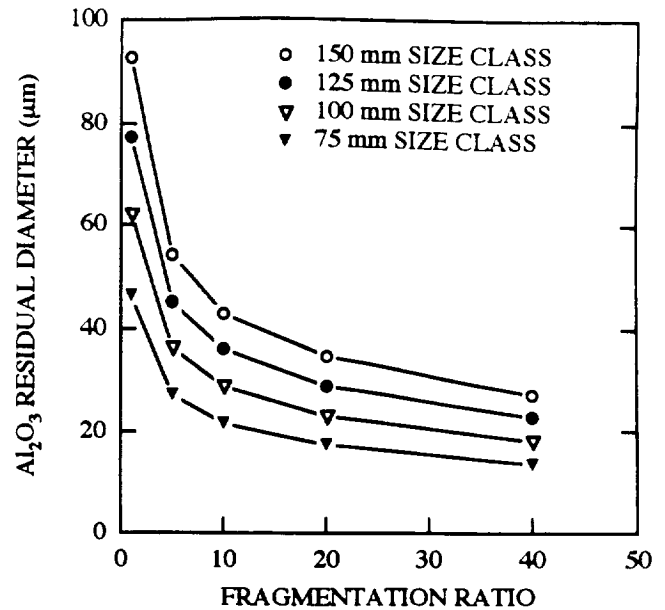


Figure 4. Final oxide residual diameter as a function of secondary atomization fragmentation ratio for a 60 wt% aluminum gel.

tion heat transfer, which has been neglected, may alter the droplet combustion process and/or the actual radiation losses. In addition, research²⁹ has indicated that the optical properties of condensed combustion products can vary considerably depending on propellant composition and oxidizer/fuel mixture ratio.

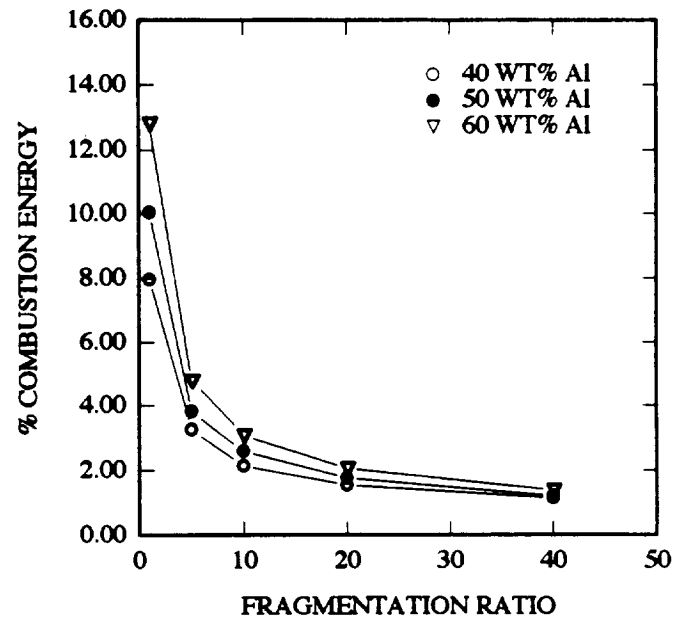


Figure 5. Radiation heat loss as a percentage of combustion energy released as a function of fragmentation ratio and gel aluminum mass loading.

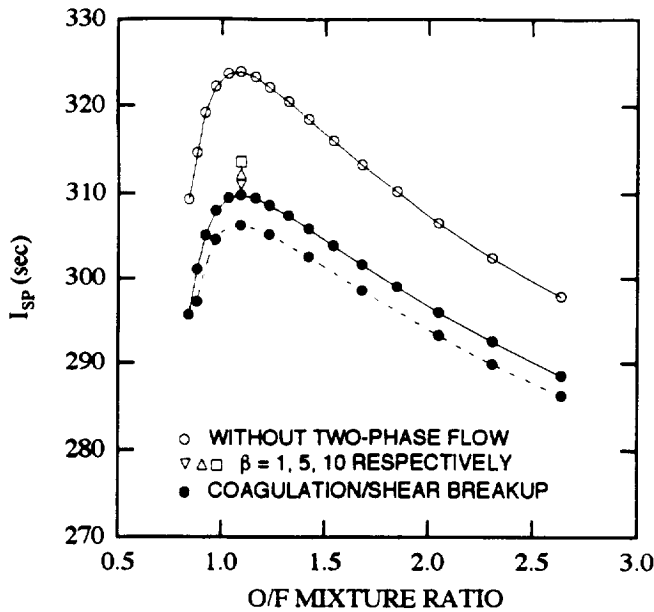


Figure 6. Engine I_{sp} as a function of oxide particle size model and O/F mixture ratio for a 60 wt% aluminum gel. Dashed line indicates inclusion of radiation losses. Model assumes an Extended Delta nozzle profile.

SPP Modeling of Engine Performance

Nozzle Two-Phase Flow

Two-phase flow effects in the engine nozzle were estimated using the SPP rocket code.²⁰ Nozzle inlet conditions were determined using a chemical equilibrium module of the SPP code that provides a mechanism to account for the radiation losses predicted by the one-dimensional combustor code.

Because particle interaction and mass transfer between the particles and gas are neglected in the SPP code, the Al_2O_3 residual size distribution predicted by the combustor code may be incorrect for nozzle performance calculations. Since the Al_2O_3 particles are molten throughout most of the nozzle, and because small particles accelerate more quickly than large particles, particle size may increase through coagulation. Similarly, additional Al_2O_3 may be produced through the recombination of gas-phase radicals as the exhaust gases cool during expansion, resulting in the nucleation of additional particles and/or growth of previously formed particles. Particle size may also decrease due to shear breakup of droplets, particularly in the throat region of the nozzle.

Because of these uncertainties in Al_2O_3 particle size, two methods of estimating particle size, which should bound the true particle size, are used in the evaluation of nozzle performance. In the first method, we use an Al_2O_3 particle size distribution that is determined by the one-dimensional combustor code, making secondary atomization the primary mechanism governing particle size. In the second method, secondary atomization is assumed to have no effect on mean particle size; rather, coagulation, parti-

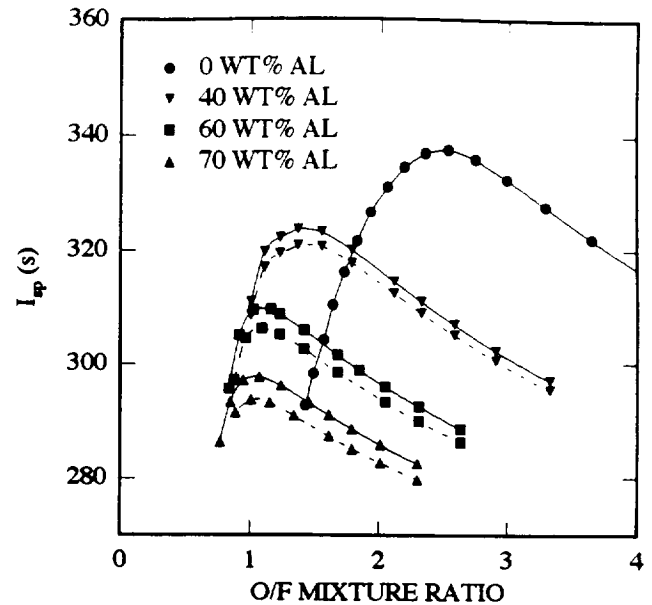


Figure 7. Engine I_{sp} as a function of O/F mixture ratio and gel aluminum mass loading. Dashed lines represent inclusion of radiation losses.

cle surface growth, and shear induced droplet breakup are assumed to be the dominant mechanisms affecting particle size. Assuming that these coagulation and breakup mechanisms are comparable to those in solid nozzles, the following solid motor correlation of mass median Al_2O_3 particle diameter, \bar{D}_{43} as a function of nozzle throat diameter was employed:²⁰

$$\bar{D}_{43} = 3.63D_t^{29/32} \quad (13)$$

This results in a particle mass median diameter of 5.6 μm .
Engine Performance Results

A comparison of two-phase flow effects on I_{sp} for the above methods of determining Al_2O_3 particle size are presented in Fig. 6 for a 60 wt% aluminum gel. As seen here, secondary atomization may reduce two-phase flow losses but not as significantly as propellant burnout distance (4% versus 62% decrease, cf. Fig. 3). To illustrate the separate contributions of radiation and two-phase flow losses, radiation losses were incorporated in the case represented by the dashed line. Given a fragmentation ratio of 5, radiation losses yield a decrease in I_{sp} of approximately 1% compared to the 4% resulting from two-phase losses.

Using the solid motor correlation for particle size, I_{sp} was calculated for a range of aluminum mass loadings and propellant mixture ratios and compared with I_{sp} calculations for a JP-10/ O_2 bi-propellant. Figure 7 shows that I_{sp} decreases with increasing aluminum loading and that the maximum I_{sp} mixture ratio becomes richer, as has been predicted by other studies,^{2,7} although the I_{sp} decrease is

much greater with the incorporation of radiation and two-phase flow losses.

Conclusions

Based on the above analysis of an Al/hydrocarbon/O₂ fueled rocket engine, the following results were obtained:

1. Exercise of the one-dimensional combustor model predicts that only moderate secondary atomization ($\beta=5$) is required to reduce overall propellant burnout distance by 62% and final Al₂O₃ residual diameter by 41%.
2. Radiation losses for a 60 wt% gel, assuming $\beta=5$, are estimated to be approximately 5 % of the energy released during combustion, resulting in a 1% decrease in engine I_{sp} . Secondary atomization may reduce radiation heat transfer losses, primarily due to decreases in the propellant burnout distance. For example, a fragmentation ratio of five results in a 61 % decrease in radiation losses. Radiation losses were also found to be a function of gel composition and engine operating conditions, as a result of changes in chamber temperature.
3. Two-dimensional, two-phase nozzle code results indicate that secondary atomization may have little effect on nozzle two-phase flow losses. Specifically, a fragmentation ratio of 5 decreases two-phase flow losses by only 4 % compared to the above 62% reduction in propellant burnout distance. Furthermore, secondary atomization may have no effect on two-phase flow losses if particle coagulation, surface growth, and shear induced breakup are the dominant mechanisms controlling oxide particle size.

Acknowledgments

This work has been sponsored by NASA-Lewis Research Center under Grant No. NAG 3-1044, with B. Palaszewski serving as technical monitor, and The Pennsylvania State University Propulsion Engineering Research Center under NASA Grant NAGW-1356.

References

1. Palaszewski, B. and Rapp, D., "Design Issues for Propulsion Systems Using Metallized Propellants". AIAA Paper 91-3424, presented at AIAA/NASA/OAI Conference on Advanced SEI Technologies, Cleveland, OH, Sept 4-6, 1991.
2. Yatsuyanagi, N., Sakamoto, H., Sato, K., Ono, F., Tamura, H., and Moro, A., "Combustion Characteristics of Metallized Hydrocarbon Fuels," 17th International Symposium on Space Technology and Science, Tokyo, Japan, May 1990.
3. Palaszewski, B., "Lunar Missions Using Advanced Chemical Propulsion: System Design Issues." AIAA Paper 90-2431, July 1990.
4. Palaszewski, B., "Metallized Propellants for the Human Exploration of Mars." NASA Technical Paper 3062, Nov. 1990.
5. Palaszewski, B., "Advanced Launch Vehicle Upper Stages Using Liquid Propulsion and Metallized Propellants." NASA Technical Memorandum 103622, Oct. 1990.
6. Palaszewski, B., and Powell, R., "Launch Vehicle Performance Using Metallized Propellants." AIAA Paper 91-2050, presented at 27th AIAA/ASME/SAE/ASEE Joint Propulsion Conference, Sacramento CA, June 1990.
7. Zurawski, R. L., and Green, J. M., "An Evaluation of Metallized Propellants Based on Vehicle Performance." AIAA Paper 87-1773, June-July 1987.
8. Schaplowsky, R. K., Anderson, R. E., Cabalet, J. A., and Vander Wall, E. M., "Characterization of Gelled RP-1 Containing Aluminum," JANNAF Propellant Development and Characterization Subcommittee Meeting, 1989.
9. Rapp, D. C., and Zurawski, R. L., "Characterization of Aluminum/RP-1 Gel Propellant Properties," AIAA Paper 88-2821, July, 1988.
10. Stearns, R. S., and Hall, L. W., Jr., "Aluminum Slurry Fuel Formulation and Combustion," AFWAL-TR-88-2052, Nov. 1988.
11. Sackheim, R. L., Huang, D. T., and Olson, A., "Mission Benefits of Liquid/Gel Propulsion for Advanced Missile Applications." Presented at AIAA Missile Sciences Conference, Naval Postgraduate School, Monterey, CA, Nov 13-15 1990.
12. Wong, S.-C., and Turns, S. R., "Ignition of Aluminum Slurry Droplets." *Combustion Science and Technology*, Vol. 52, 1987, pp. 222-242.
13. Turns, S. R., Wong, S.-C., and Ryba, E., "Combustion of Aluminum-Based Slurry Agglomerates," *Combustion Science, and Technology*, Vol. 54, 1987, pp. 299-318.
14. Clausen, L. C., Li, T. X., and Law, C. K., "Effects of Additives on the Microexplosion of Carbon Slurry Droplets," *AIAA Journal Of Propulsion and Power*, Vol. 4, pp. 217-221.
15. Wong, S. -C., and Turns, S. R., "Disruptive Burning of Aluminum/Carbon Slurry Droplets." *Combustion Science and Technology*, Vol. 66, 1989, pp. 299-318.
16. Wong, S.,-C., A.-C. and Chi, H.,-Y., "Effects of Surfactant on the Evaporation, Shell Formation, and Disruptive Behaviors of Slurry Droplets." Twenty-Third Symposium (International) on Combustion, The Combustion Institute, Pittsburgh, 1990, pp. 1391-1397.
17. Cho, S. Y., Takahashi, F., and Dryer, F. L., "Some Theoretical Considerations on the Combustion and Disruption of Free Slurry Droplets." *Combustion Science and Technology*, Vol. 67, 1989, pp. 37-57.
18. Lee, A., and Law, C. K., "Gasification and Shell Characteristics in Slurry Droplet Burning," *Combustion and Flame*, Vol. 85, 1991, pp. 77-93.

19. Mueller, D. C., and Turns, S. R., "Some Aspects of Secondary Atomization of Aluminum/Hydrocarbon Slurry Propellants," *ALAA Journal of Propulsion and Power*, Vol. 9, May-June 1993, pp. 345-352.
20. Nickerson, G.R., et. al., "The Solid Propellant Rocket Motor Performance Prediction Computer Program (SPP), Version 6.0." AFAL/TSTR, Edwards AFB, CA, Dec 1987.
21. Kraeutle, K.J., "Particle Size Analysis in Solid Propellant Combustion Research," *Progress in Astronautics and Aeronautics*, Vol. 53, 1977, pp. 449-463.
22. Salita, M., "Quench Bomb Investigation of Al₂O₃ Formation From Solid Rocket Propellants (Part II): Analysis of Data." 25th JANNAF Combustion Meeting, Oct. 1988, pp. 185-197.
23. Parry, D. L., and Brewster, M. Q., "Optical Constants of Al₂O₃ Smoke," *Journal of Thermophysics*, Vol. 5, April-June 1991, pp. 142-149.
24. Siegel, R., and Howell, J. R., Thermal Radiation Heat Transfer-Second Edition, Hemisphere Publishing Corp., New York, 1981.
25. Turns, S. R., and Mueller, D. C., "Ignition and Combustion of Metallized Propellants: Final Report- Phase I," to NASA-Lewis Research Center Grant No. NAG 3-1044, Jan 1993.
26. Faeth, G. M., "Current Status of Droplet and Liquid Combustion," *Prog. Energy Combust. Sci.*, Vol. 3, 1977, pp. 191-224.
27. Law, C. K., and Williams, F. A., "Kinetics and Convection in the Combustion of Alkane Droplets," *Combustion and Flame*, Vol. 19, 1972, pp. 393-405.
28. Anon., IMSL Library Reference Manual, IMSL, Inc., January 1, 1982.
29. Konopka, W. L., Reed, R. A., and Calia, V. S., "Measurements of Infrared Optical Properties of Al₂O₃ Rocket Particles," *Progress in Astronautics and Aeronautics*, Vol. 91, AIAA, New York, 1984, pp. 180-196.
30. Mueller, D. C., and Turns, S. R., "Ignition and Combustion of Metallized Propellants- Annual Report," to NASA-Lewis Research Center, Grant No. NAG 3-1044, Aug 1992.